IEEE Open Journal of Nanotechnology

Received 5 September 2022; revised 10 November 2022 and 9 December 2022; accepted 19 December 2022. Date of publication 22 December 2022; date of current version 5 January 2023. The review of this article was arranged by Associate Editor Atsuhiko Fukuyama.

Digital Object Identifier 10.1109/OJNANO.2022.3231436

Transition Metal Doped Bismuthene and Mn-Bi/CrI_3 Heterostructure for High Anisotropy Energy and Half-Metallicity

SHIPRA SAINI, NAMITA BINDAL, AND BRAJESH KUMAR KAUSHIK (Senior Member, IEEE)

Department of Electronics and Communication Engineering, Indian Institute of Technology Roorkee, Roorkee 247667, India

CORRESPONDING AUTHOR: BRAJESH KUMAR KAUSHIK (email: bkk23fec@iitr.ac.in)

ABSTRACT Magnetic anisotropy energy (MAE) of two-dimensional (2D) magnetic materials is the key parameter for designing next-generation spintronic devices. Here, using first-principle calculations based on density functional theory (DFT), the variance in MAE and other magnetic properties is observed for transition metal (TM) doped bismuth monolayer (bismuthene). This doped system shows a significant modulation in the magnetic moment, MAE, Curie temperature T_c, and charge transfer. However, Mn-doped bismuthene exhibits half-metallicity with a maximum magnetic moment of 4μB (Bohr magneton) that is 17% higher than Fe-doped bismuthene. The maximum MAE extracted for Mn-doped bismuthene is 27.51% higher than the Ti-doped system. On the basis of these findings, the electronic and magnetic characteristics of Mn-doped bismuthene (Mn-Bi) and monolayer CrI_3 van der Waals (vdW) heterostructures are also investigated. In Mn-Bi/CrI_3 van der Waals heterostructure, the half-metal Mn-Bi can induce the half-metallicity in CrI_3 through charge transfer. Compared to other doped systems, Mn-Bi presents the most favorable magnetic properties. Thus, Mn-Bi/CrI_3 heterostructure paves the path for the development of spintronic devices.

INDEX TERMS Bismuthene, density functional theory, magnetic anisotropy energy, substitutional doping, 2D materials, spin-orbit coupling, heterostructure.

I. INTRODUCTION

The involvement of magnetism in 2D materials has attracted considerable interest for use in spintronic devices. However, most of the 2D materials lack inherent spin polarization owing to the fact that the non-magnetic components make up their structures that significantly limits their direct use in spintronics. It is still difficult to prepare the ferromagnetic 2D materials with high MAE to perform experiments above the room temperature [1]. Hence, it would be ideal to opt for a novel material exhibiting both unique electronic and magnetic properties. Currently, numerous techniques including vacancy defects, doping, strain, and chemical functionalization [2], [3] can be used to generate the magnetism in 2D materials. Among these, doping with TM atoms is considered as a conventional and simple method to modify the electronic and magnetic characteristics of 2D materials [4]. A small fraction of TM atoms doped into a 2D host material causes magnetic ordering. The interactions that determine whether a material will exhibit ferromagnetic or antiferromagnetic behavior are influenced by the orbital overlap of the unpaired d states of the TM. In the past, theoretical simulations have shown that the $4d$ and $5d$ TM impurities can impart magnetism into the graphene nanosheet.

In 2013, Cheng et al. discovered that doping TMs in the monolayer MoS_2 can produce diluted magnetic semiconductor (DMS) [5]. Additionally, numerous studies have shown that doping of TMs in the phosphorene, arsenene, and antimonene exhibits half metallicity and considerable MAE in addition to being able to supply a controllable magnetic moment [6], [7]. The nitrogen group has been studied, and it is discovered that the heaviest element in group 15 is bismuth [8]. Each bismuth (Bi) atom in bismuthene links covalently to its three closest neighbors in a honeycomb-like arrangement. Owing to the features such as high structural properties, thermal stability, and wide band gap, bismuthene has gained considerable interest. Molecular dynamics analysis shows that bismuthene is resistant at high temperatures, thus revealing the mechanical stability of bismuthene [9]. In order to make

bismuthene a potential candidate for spintronic applications, intrinsic non-magnetic state can be doped with magnetically active TM dopants. Moreover, single-layer chromium trihalides CrX_3 (X = F, Cl, Br, I) are stable, ferromagnetic, and retain their intrinsic magnetism under elastic tensile strain [10]. Atomically thin CrI_3 acts as a spin-filter tunnel barrier for multiple-spin-filter magnetic tunnel junctions (sf-MTJs) based on van der Waals (vdW) heterostructures [11]. Notably, the simple assembly of 2D Vander Waals (vdW) crystals has drawn a lot of attention to vdW spintronic devices.

In this work, the MAE, magnetic moment, charge transfer, and other properties of TM (Ti, Cr, Fe, Mn, and Co) doped bismuthene using DFT are investigated. It is observed that Mn significantly modulates the properties of bismuthene. Later on, the electronic and magnetic properties of a single layer of CrI_3 and Mn-Bi/CrI_3 heterostructure are investigated using DFT. These calculations demonstrate that the Mn-Bi monolayer is half-metal and CrI_3 is an intrinsic ferromagnetic semiconductor with a band gap of 1.3 eV. However, charge transfer causes CrI_3 to become half-metallic in the heterostructure. The spin polarizations of the electrodes are all very close to 100% due to the half-metallic characteristics of the monolayer Mn-Bi and Mn-Bi/CrI_3 heterostructures.

The rest of the paper is organized as follows: Section II describes the computational setup used for the analysis of different magnetic properties of bismuthene. Section III highlights the results and analysis of magnetic moment, MAE, T_c, and electronic stability of TM doped bismuthene as well Mn-Bi/CrI_3 heterostructure. Section IV discusses the conclusions of TM doped bismuthene and half-metallic electrodes.

II. COMPUTATIONAL DETAILS

DFT framework is used to analyze the structural, magnetic, and electronic characteristics of pure and doped bismuthene on the atomistix toolkit (ATK) simulator [12]. To represent the exchange-correlation potential, the Perdew-Burke-Ernzerhof (PBE) of the generalized gradient approximation (GGA) functional is employed [13]. Bismuthene is arranged in a 4x4x1 supercell with a vacuum gap of 20 Å along the z-axis in order to prevent interaction between the nearby layers. The gradient convergence and step size are considered as 0.02 eV/Å and 0.001Å, respectively. The structures are geometrically optimized with self-consistent field (SCF) convergence without any symmetry constraints. The doped bismuthene contains 31 bismuth atoms and one dopant atom having a doping concentration of 3.125%. After the second atom is doped into the bismuthene, the concentration rises to 6.25%. To analyze the electronic and magnetic properties of intrinsic and TM doped bismuthene, spin polarization is used throughout all calculations. The top and side views of the 4x4x1 supercell of bismuthene are shown in Fig. 1(a) and (b), respectively. The bismuth atoms have the configuration of $6s^2\ 6p^3$ for valence electron. However, the dopant atom including Ti, Cr, Mn, Fe, and Co has valence electron configuration of $3d^24s^2$, $3d^54s^1$, $3d^54s^2$, $3d^64s^2$, and $3d^74s^2$, respectively. For the structural relaxation calculations, the *k*-point sample for Brillouin zone

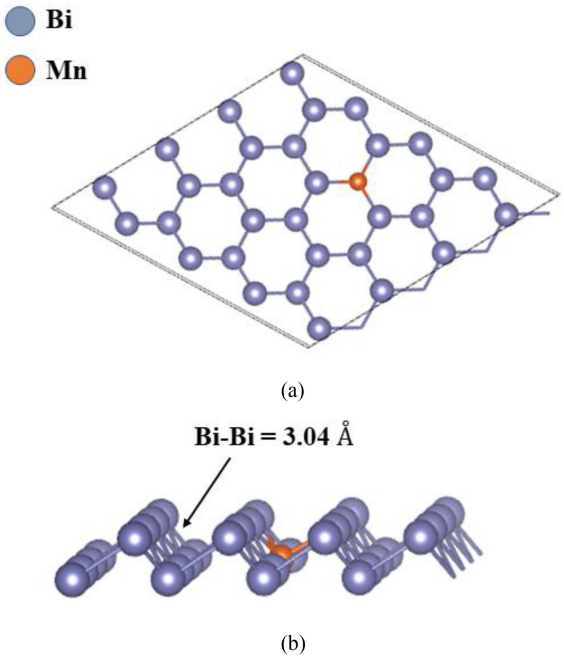

FIGURE 1. Optimized structure of TM doped bismuthene 4x4x1 super cell (a) top view and (b) side view. Here, Mn is considered as a dopant atom.

integration is considered as 7x7x1 with the Monkhorst-Pack grid [14]. The density mesh cut-off in a linear combination of atomic orbitals (LCAO) calculator is set to be 225 *Hartree* for plane wave expansion of wave function and 1000 *K* for broadening.

For band gap and density of states calculations, mean-field Hubbard correction (DFT+*U*) is used. Here, *U* is an additional energy *E* term in exchange-correlation. The essential assumption for strongly correlated *d* orbital electrons is subject to onsite quasi-atomic interactions. The Hubbard parameter *U* is defined as follows [15]:

$$U = E\left(d^{n+1}\right) + E\left(d^{n-1}\right) - 2E\left(d^{n}\right) \tag{1}$$

This is the coulomb energy cost to place two electrons at the same site. Most often, GGA+PBE underestimates the band gap of the materials. Moreover, the band structure of the TM-doped bismuthene and Mn-Bi/CrI_3 heterostructure are also calculated by the HSE06. The charge transfer estimates the charge on interacting donor and acceptor atoms. This is done by employing the Mulliken population that allows to calculate the net difference of spin-up and spin-down states. Moreover, the charge difference density and spin distribution are also analyzed to study the charge transfer and other magnetic properties.

III. RESULTS AND DISCUSSIONS

To envision the magnetic properties of 2D materials and their vdW interactions, computations are done to analyze the intrinsic, TM doped bismuth monolayer, and Mn-Bi/CrI_3 heterostructure. The computation of results related to structure,

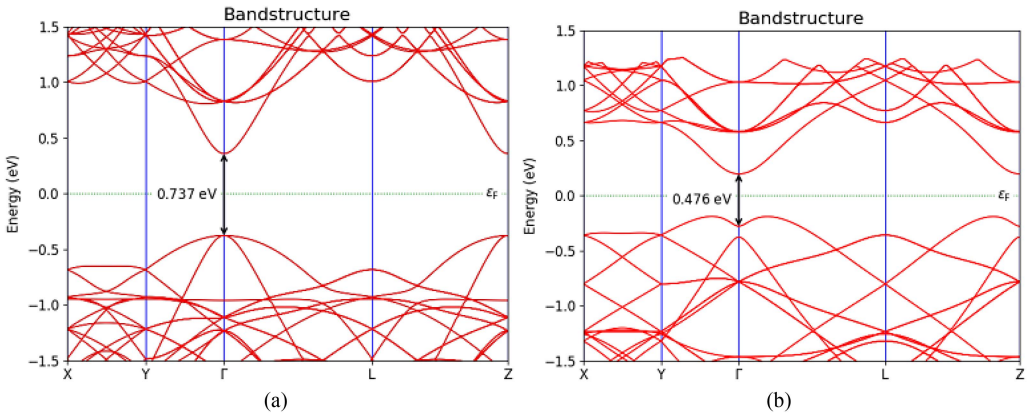

FIGURE 2. Band structure plot for pristine bismuthene (a) without SOC and (b) with SOC using PBE+U.

TABLE 1. Estimation of the Bond Length, Binding Energy, and Bandgap of Doped Bismuthene With Different Transition Dopant Atoms

Bismuthene monolayer	Bond length (Å)	Binding energy (eV)	Bandgap (eV)	Characteristics
Intrinsic	3.04	-4.657	0.737	Non-magnetic insulator
Ti-doped	2.86	-2.915	0.133	Magnetic semiconductor
Cr-doped	2.83	-1.101	0.235	Magnetic semiconductor
Mn-doped	2.86	-3.901	0	Half metal
Fe-doped	2.70	-1.373	0	Magnetic metal
Co-doped	2.77	-2.816	0	Magnetic metal

magnetic properties, and charge transfer are described in the following sub-sections.

A. CRYSTAL STRUCTURE AND LATTICE DYNAMICS

The crystal structure of buckled Bi monolayer is hexagonal and a fully relaxed supercell size of 4 × 4 × 1 periodicity is used in this work. The crystal structure of Bi monolayer has the lattice constants $a = b = 4.36$ Å and $c = 12.17$ Å. In pristine Bi monolayer, the covalent bond length (Bi-Bi) and the buckling height are observed as 3.04 Å and 1.68 Å, respectively. These values match the previous theoretical and experimental results [16]. Following substitutional doping, it is seen that the covalent bond length between the bismuth atoms and the transition metal dopant atoms varies. These variations are due to different atomic sizes of the dopant atoms that lead to lattice distortions and inter-atomic interactions. These covalent bonds have shorter lengths than the one that exists between the two bismuth atoms (Bi-Bi).

Table 1 presents the bond length between the dopant and bismuth atom, binding energy and bandgap of different TM doped bismuthene monolayer. The smallest bond length of 2.70 Å is observed for Fe-doped bismuthene. Using PBE+U, the bandgap of 0.737 eV is obtained for pristine bismuthene. By considering the SOC, the bandgap is reduced to 0.476 eV as shown in Fig. 2. However, with HSE06, the bandgap is obtained 1.2 eV without SOC effect and the bandgap is nearly equal with HSE06 and PBE with SOC as shown in Fig. 3. It is also observed that there is spin dependence in the band structure: the up and down states are degenerating. Otherwise, both the blue and red curves will be observed in the same band structure plot.

TABLE 2. Different Magnetic Parameters of Doped Bismuthene System

Dopant Atom (X)	Ti	Cr	Mn	Fe	Co
Magnetic moment (μ_B)	2.28	3.14	4.01	3.42	2.39
MAE (meV)	8.36	-5.71	10.66	-7.98	-9.12
Corrected T_c (K)	102	160	479	49	326

B. MAGNETIC MOMENT AND MAE OF DOPED BISMUTHENE

The difference in moments between the two spin states (up and down) is known as the total magnetic moment. However, each doped atom independently makes up the local magnetic moment. The MAE property, regarded as the magnetization direction-dependent factor is crucial in determining the magnetic nature. The MAE is caused by the splitting of higher energy 3*d* orbitals such as d_{xy}, $d_{x^2-y^2}$, and d_{yz} of dopant atoms, and it can be defined as follows [17]:

$$MAE = E_X - E_Y \tag{2}$$

where, E_X and E_Y are the energies corresponding to in-plane and out-of-plane magnetization directions. The out-of-plane (in-plane) magnetization direction is preferred, as indicated by the positive (negative) MAE. Mn-doped system has a higher magnetic moment and MAE in comparison to other monolayer systems. However, Co-doped bismuthene has −9.12 meV indicating the in-plane magnetization direction. Table 2 presents the estimated values of magnetic moment and MAE along with T_c discussed in the next subsection.

C. CURIE TEMPERATURE

Curie temperature (T_c) of doped bismuthene can be calculated with the help of MAE. The higher the MAE, the higher will

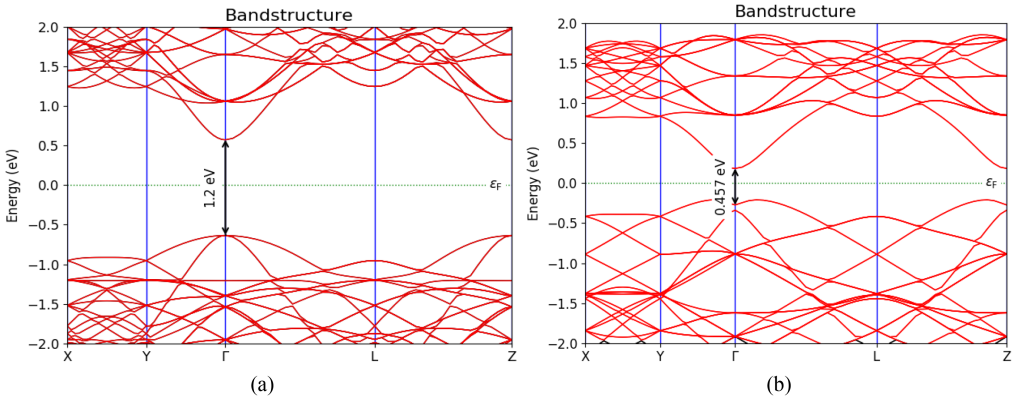

FIGURE 3. **Band structure plots for pristine bismuthene (a) without SOC and (b) with SOC using HSE06.**

be T_c [18]. According to the mean-field theory (MFT), T_c can be expressed as follows [19]:

$$T_c = \frac{2}{3K_B}(-\Delta E) \tag{3}$$

where, K_B *is* Boltzmann's constant. ΔE is the difference in the energy between ferromagnetic and antiferromagnetic states, respectively. The MFT overestimates the value of T_c, hence a correction factor is used to calculate the exact value that is represented as follows [20]:

$$T_c\,(corrected) = 0.506 * T_c\,(MFT) \tag{4}$$

The Mn-doped bismuthene has the corrected T_c as 479K and Fe-doped has the lowest T_c in comparison to all other systems studied here.

D. ELECTRONIC STABILITY AND CHARGE TRANSFER IN 3D ORBITALS OF DOPED ATOMS IN BISMUTHENE AND MN-BI/CRI$_3$ VAN DER WAALS HETEROSTRUCTURE

The stability of TM doped bismuth monolayer can be predicted using binding energy (E_b) that is expressed as follows [21]:

$$E_b = (E_{Doped} - E_{TM} - E_{Bi}) \tag{5}$$

where, E_{Doped} is the total energy of the TM-doped Bi monolayer, E_{TM} and E_{Bi} are the energies of free TM dopant atom and bismuth atom, respectively. It is observed that the binding energies for all the TM-doped monolayers are negative, illustrating that all the TM-doped Bi monolayers are stable. However, Mn doped Bi monolayer has the lowest binding energy (as shown in Table 1), indicating the most stable monolayer among other TM-doped Bi monolayers. It is evident from the substitutional doping of 3d TM in the bismuth monolayer that the magnetic and electronic characteristics of the doped system have undergone considerable modifications. This change is due to the unpaired electron in *3d* orbitals of the doped atom. The 3*d* orbital includes five degenerate levels which are d_{xy}, $d_{x^2-y^2}$, d_{yz}, d_{z^2}, and d_{xz}. The degeneracy is divided into energy levels that make up orbitals that are either bonding or antibonding. Bonding orbitals that are formed with lower energy have filled electrons and hence, do not participate in charge transfer. Charge transfer happens because of the distribution of the electrons, which is carried out via the high energy antibonding orbitals. The charge transfer in various degenerate levels of 3*d* orbitals is shown in Table 3. The spin-up and spin-down states are represented by $\mu_\uparrow$ and $\mu_\downarrow$, respectively. It can be seen that the Mn-doped system shows the maximum variation in spin-up and spin-down states, particularly highest for orbitals $d_{x^2-y^2}$ and d_{xy}. It is worth noting that there are significant changes in charge distribution for different doped bismuth monolayers. These variations can also be seen with the help of local density of states (LDOS) as shown in Fig. 4. From Fig. 4(a), it is visible that no states are available at the fermi level that can be occupied by spin-up or spin-down electrons in pristine bismuthene. However, as shown in Fig. 4(b), Mn-doped system has partially filled states at fermi level thus indicating the metallic nature. The band structure and PDOS of Mn-doped system are shown in Figs. 6(a) and 7(a), respectively. It should be noted that the spin-up bands pass the fermi level, whilst the spin-down channel behaves as a semiconductor, showing that it is an intrinsic half-metallic material with a 100% spin polarization ratio. The half-metallic gap for this system is 0.375 eV and spin gap for semiconducting channel is 0.864 eV. Half-metallic gap (semi-metal gap) is defined as the difference between Fermi level and the valence band maximum of minority spin sub-band (spin down band). The half-metallic gap influences the ability of the half-metal to resist thermal fluctuations. To achieve promising applications for half-metallics in spintronic devices, wide half-metallic gaps are extremely important. The larger the half-metallic gap, the larger is the bias voltage required to generate the tunneling current, and correspondingly, the better its ability to maintain the high TMR [11]. For any spintronic device to work better and be used in spintronics-based applications, high spin injection efficiency and tunneling magnetoresistance is necessary. Half-metallic ferromagnets with 100% spin polarization can be used as electrodes to meet the aforementioned specifications. It is actually difficult to form half-metal heterojunctions by doping; therefore, we constructed a new half-metallic heterostructure based on the charge

TABLE 3. Charge Distribution of 3D Orbitals in Transition Metal Doped Bismuthene

Doped system	Spin-up and spin-down states	d_{xy}	$d_{x^2-y^2}$	d_{xz}	d_{yz}
Ti-doped	$\mu_\uparrow$	0.445	0.441	0.442	0.435
	$\mu\downarrow$	0.131	0.131	0.144	0.144
Cr-doped	$\mu_\uparrow$	0.848	0.848	0.863	0.863
	$\mu\downarrow$	0.018	0.018	0.017	0.018
Mn-doped	$\mu_\uparrow$	0.951	0.950	0.952	0.952
	$\mu\downarrow$	0.112	0.114	0.127	0.127
Fe-doped	$\mu_\uparrow$	0.941	0.940	0.953	0.953
	$\mu\downarrow$	0.313	0.312	0.314	0.134
Co-doped	$\mu_\uparrow$	0.958	0.958	0.970	0.953
	$\mu\downarrow$	0.646	0.627	0.516	0.490

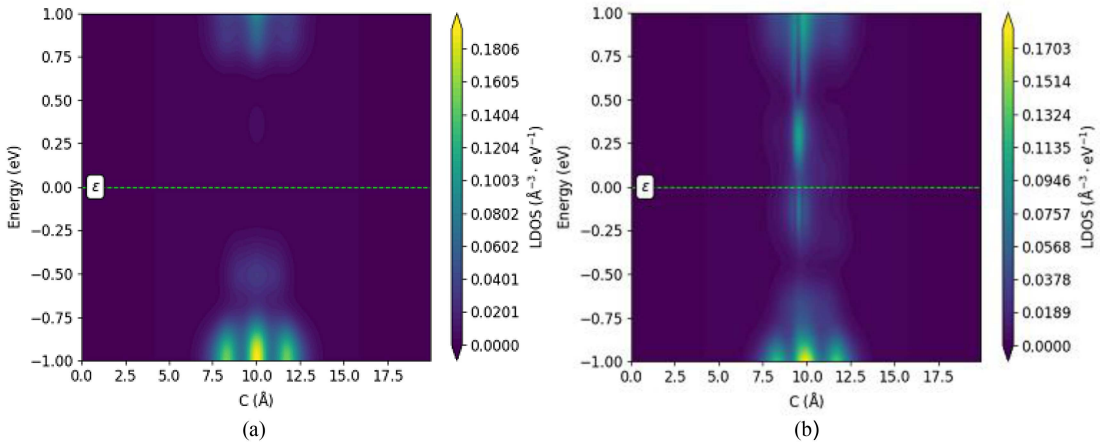

FIGURE 4. LDOS plots for (a) Pristine (b) Mn-doped bismuthene where C is distance along z direction.

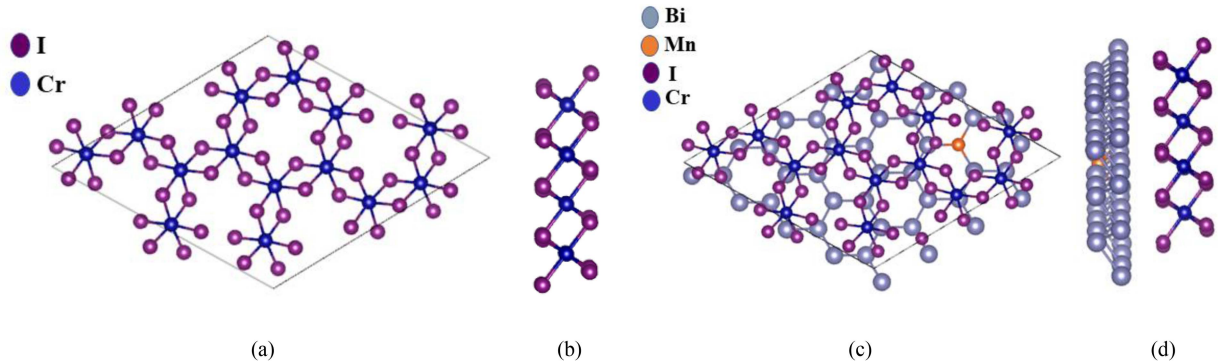

FIGURE 5. (a) Top view and (b) Side view of CrI_3, (c) Top view and (d) Side view of Bi-Mn/CrI_3 heterostructure.

transfer-induced half-metallic properties that can be used as a magnetic tunnel junction electrode. And two-dimensional (2D) materials have the ability to form heterostructures without the need for lattice matching. The Mn-Bi/CrI_3 heterostructure is fully optimized with minimum lattice mismatch. This heterostructure has the mean absolute strain of 0.58%, thus indicating the small effect of strain on its electronic structure [22]. CrI_3 can be used as a magnetic tunnel barrier for vdW heterostructure spintronic devices. However, the spins align ferromagnetically out-of-plane within each layer but antiferromagnetically between layers, resulting in vanishing net magnetization [23]. But, its heterostructure with

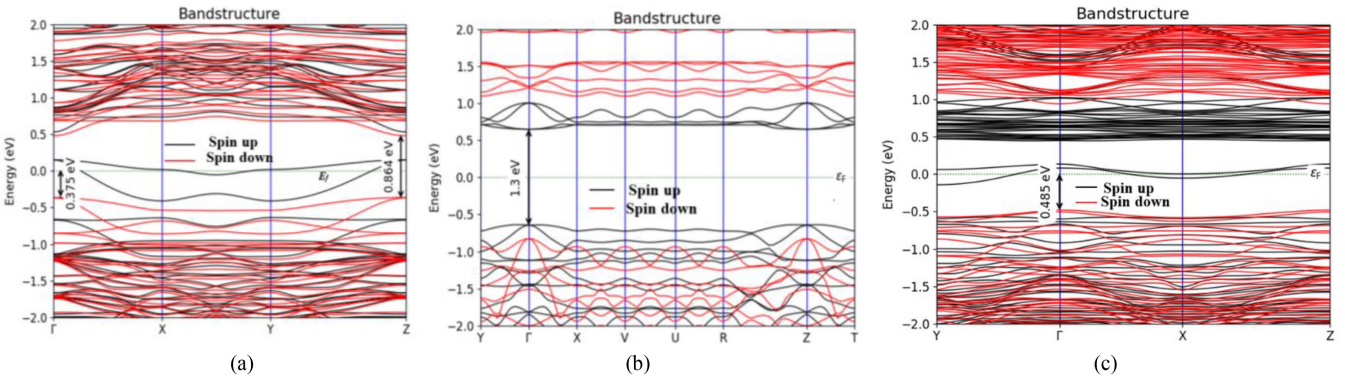

FIGURE 6. **Bandstructure plot of (a) Bi-Mn monolayer, (b) CrI_3 monolayer, and (c) Bi-Mn/CrI_3 heterostructure.**

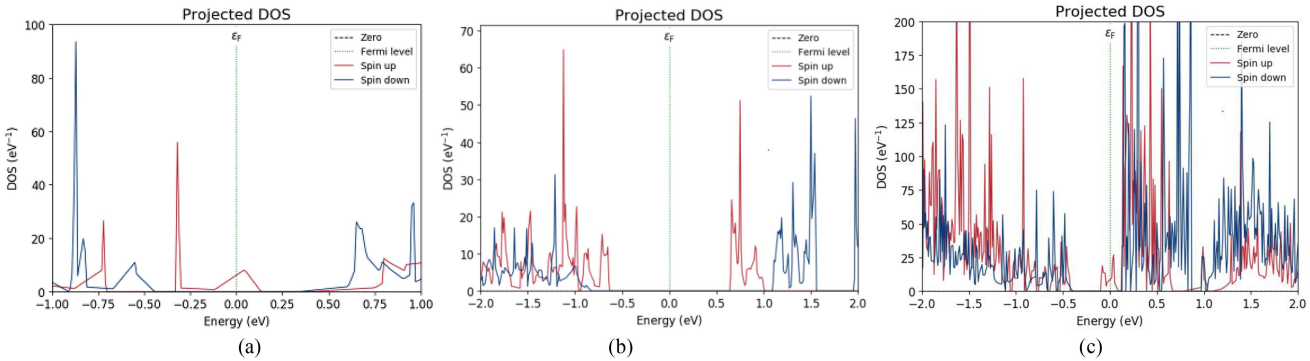

FIGURE 7. **PDOS plots of (a) Bi-Mn monolayer, (b) CrI_3 monolayer, and (c) Bi-Mn/CrI_3 heterostructure. Here, red color presents spin up states while blue color is presenting spin down states.**

TABLE 4. **Binding Energies and Interlayer Distances for Heterostructurs**

Interlayer distance (Å)	3.11	3.18	3.72	4.12	4.97
Binding Energy E_b (eV/atom)	-1.56	-1.61	-1.65	-1.64	-1.63

Mn-doped bismuthene embeds the half-metallicity in CrI_3 monolayer. However, the binding energy of the Mn-Bi/CrI_3 heterostructure is estimated as -1.65 eV at 3.72 Å vdW interlayer distance. Fig. 5 presents the top and side views of the monolayer CrI_3 and Mn-Bi/CrI_3 vdW heterostructure. Fig. 6(b) shows the band structure of monolayer CrI_3 which is a magnetic insulator. The band structure and PDOS plot for the heterostructure is presented in Figs. 6(c) and 7(c), respectively with 0.485 eV half-metallic gap. This indicates the half-metallicity in the heterostructure that is caused by the charge transfer between Mn-Bi and CrI_3 monolayers. Table 4 illustrates the binding energy of the heterostructure at different inter-layer distances. It is observed that with interlayer distance 3.72 Å, the heterostructure is most stable as binding energy is minimum.

To study the further magnetic properties, the spin density distribution of Mn-doped bismuthene and Mn-Bi/CrI_3 heterostructure are performed. Figs. 8 and 9 depicts that the charge density difference of Mn doped Bi monolayer and CrI_3 monolayer. Here, the yellow color represents an accumulation in the charge density, while green color indicates the depletion in the charge density. Figs. 8(c) and 9(c) shows the charge density difference Mn-Bi/CrI_3 heterostructure. Figs. 10 and 11 shows the top view and side view of the spin density distribution of Mn doped Bi monolayer, CrI_3 and their heterostructure, respectively. The Bader Charge analysis algorithm, developed by Henkelman [24], is used to calculate charge transfer. The transferred charge between the Mn-doped Bi monolayer and the CrI_3 monolayer is obtained using the following equation [25]:

$$\Delta q = q_{after} - q_{before} \tag{6}$$

where, Δq is the difference in Bader charges of CrI_3 monolayer after (q_{after}) and before (q_{before}) the heterostructure formation. Bader charge analysis reveals that a charge about 1.02 electron (e) transferred from the Mn-doped Bi monolayer to the CrI_3 monolayer. Table 5 shows the total charges on individual monolayers and Mn-Bi/CrI_3 heterostructure

The half-metallic gap is the key factor affecting the spin injection efficiency and tunnel magnetoresistance of

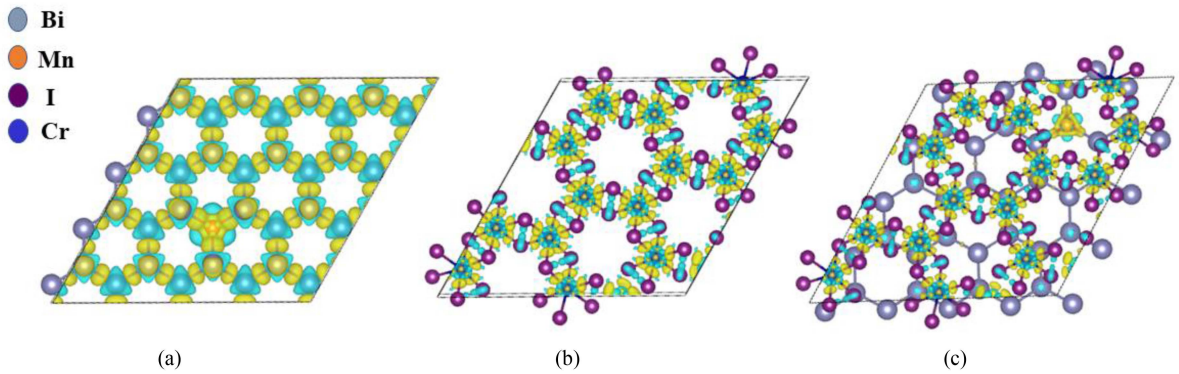

FIGURE 8. The top view of charge density difference of (a) Mn doped Bi monolayer, (b) CrI_3 monolayer, and (c) Mn-Bi/CrI_3 heterostructure. Here the yellow color represents an accumulation in the charge density, while green color indicates the depletion in the charge density.

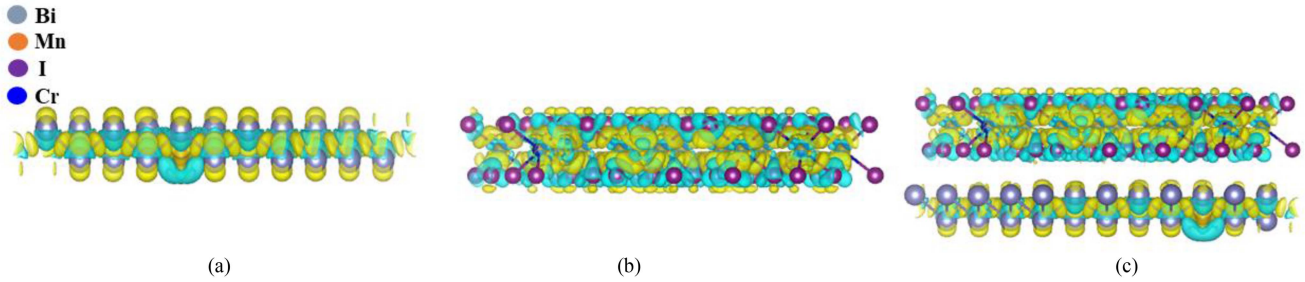

FIGURE 9. The side view charge density difference of (a) Mn doped Bi monolayer, (b) CrI_3 monolayer, and (c) Mn-Bi/CrI_3 heterostructure Here the yellow color represents an accumulation in the charge density, while green color indicates the depletion in the charge density.

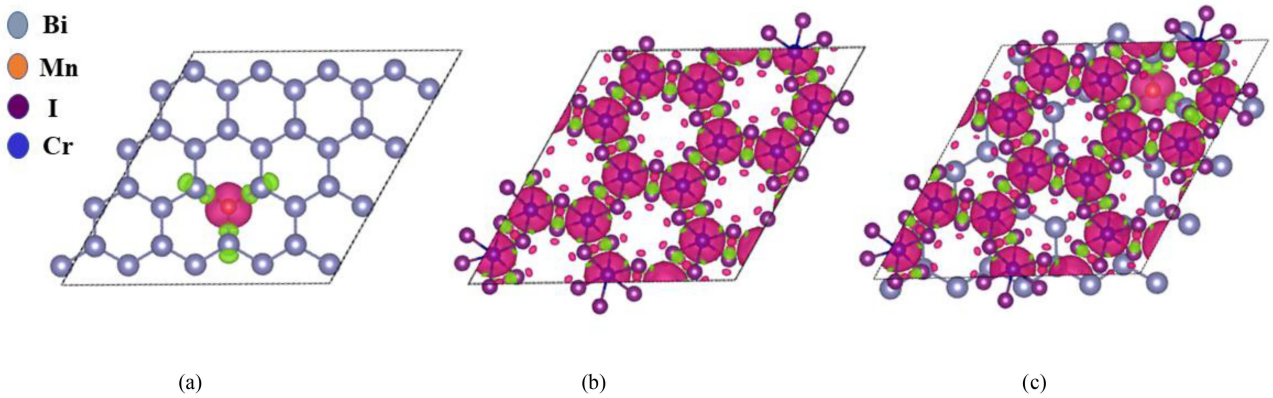

FIGURE 10. The top view of spin density distribution of (a) Mn doped Bi monolayer, (b) CrI_3 monolayer, and (c) Mn-Bi/CrI_3 heterostructure. The pink (green) color corresponds to a positive (negative) value, where a positive value is attained whenever spin up is more than spin down and vice-versa.

half-metallic electrode magnetic tunnel junction. A half-metal/insulator/half-metal magnetic tunnel junction [26] can be created based on the interlayer charge transfer effect in vdW Mn-Bi/CrI_3 heterojunctions.

Spin injection efficiency (η) can be expressed as follows [27]:

$$\eta = \frac{I(\uparrow) - I(\downarrow)}{I(\uparrow) + I(\downarrow)} \tag{7}$$

where, I(↑) and I(↓) are the current obtained in parallel and anti-parallel configuration. Negligible current is obtained in antiparallel configuration because 100% spin polarization in half-metal electrode only enables one form of spin to flow through the channel and inhibits other types of spin. The Mn-doped bismuthene shows better metrics in terms of magnetic moment, MAE, and Tc when compared to other doped systems as shown in Table 6.

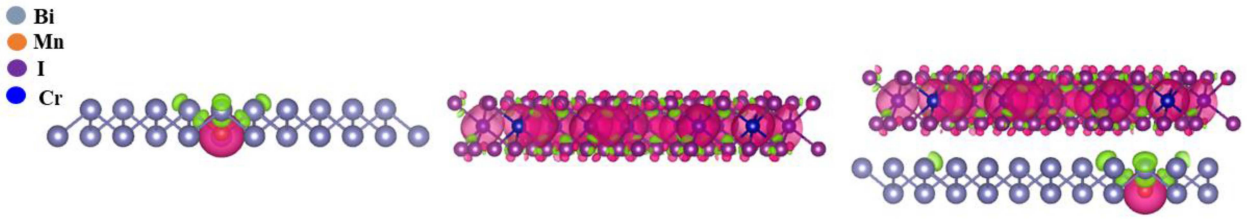

FIGURE 11. The side view of spin density distribution of (a) Mn doped Bi monolayer, (b) CrI_3 monolayer, and (c) Mn-Bi/CrI_3 heterostructure. The pink (green) color corresponds to a positive (negative) value, where a positive value is attained whenever spin up is more than spin down and vice-versa.

TABLE 5. Bader Analysis for Different Monolayers and Their Heterostructure

Systems	Total charge (e)
Bi monolayer	217.76
Mn-doped Bi monolayer	215.33
CrI_3 monolayer	377.71
Mn-Bi/CrI_3 heterostructure	592.96

TABLE 6. Comparison of Transition Metal Doped Bismuthene With Other Doped System

Doped system	MAE (meV)	Magnetic moment (μB)
Mn-MoS_2 [28]	8.46	3.419
Mn- $MoSe_2$ [28]	8.25	1.401
Fe- MoS_2 [29]	5.05	1.379
Co- MoS_2 [30]	3.58	3
Fe-InP_3 [21]	0.34	5
Co-Phosphorene [31]	-10.26	1.24
Mn-bismuthene [This work]	10.66	4.01

IV. CONCLUSION

The optimized configurations of TM doped bismuthene systems, monolayer CrI_3 and Mn-Bi/CrI_3 heterostructure are studied using DFT for magnetic and electronic properties. It is worthy to note that the Mn-doped bismuth monolayer exhibits favorable magnetic properties including magnetic moment, MAE, T_c, and half-metallicity. The charge transfer variations are significant for $d_{xz}$and d_{xy} orbitals for the spin-up and spin-down states as compared to $d_{x^2-y^2}$ orbitals. The total magnetic moment of Mn-Bi is much higher than Mn-MoS_2 and Fe-doped bismuthene by 14.74% and 17.25%, respectively. Furthermore, the Mn-doped system has the highest T_c when compared with other TM doped bismuthene. The maximum MAE extracted for half-metallic Mn-Bi is 20.63% higher than Mn-MoS_2. While studying the Mn-Bi/CrI_3 heterostructure, it is observed that the CrI_3 layer switches to the FM half-metal owing to the electron transfer. The half-metallic gap of the heterostructure is 0.485 eV. This shows that Mn-Bi/CrI_3 half-metallic electrode exhibits more robust magnetic properties, thus paving the way for designing the next-generation spintronic devices.

REFERENCES

[1] R. L. Han, Z. Jiang, and Y. Yan, "Prediction of novel 2D intrinsic ferromagnetic materials with high curie temperature and large perpendicular magnetic anisotropy," *J. Phys. Chem.*, vol. 124, no. 1, pp. 7956–7964, 2020.
[2] Y. G. Zhou et al., "Tensile strain switched ferromagnetism in layered NbS2 and NbSe2," *ACS Nano*, vol. 6, no. 1. pp. 9727–9736, 2012.
[3] S. Radhakrishnan et al., "Fluorinated h-BN as a magnetic semiconductor," *Sci. Adv.*, vol. 3, 2012, Art. no. e1700842.
[4] S. Saini and S. Choudhary, "Spin investigation in transition metal doped two-dimensional bismuth (bismuthene) for use in spintronics applications," *Adv. Natural Sci.: Nanosci. Nanotechnol.*, vol. 13, no. 1, pp. 1–7, 2022.
[5] Y. C. Cheng, Z. Y. Zhu, W. B. Mi, Z. B. Guo, and U. Schwingenschlogl, "Prediction of two-dimensional diluted magnetic semiconductors: Doped monolayer MoS2 systems," *Phys. Rev. B*, vol. 87, no. 1. 2013, Art. no. 100401.
[6] X. Gonze, J. P. Michenaud, and J. P. Vigneron, "First-principles study of As, Sb, and Bi electronic properties," *Phys. Rev. B*, vol. 41, no. 17, 1990, Art. no. 11827.
[7] M. Pumera and Z. Sofer, "2D monoelemental arsenene, antimonene, and bismuthene: Beyond black phosphorus," *Adv. Mater.*, vol. 29, no. 21, 2017, Art. no. 1605299.
[8] S. Zhang et al., "Atomically thin arsenene and antimonene; semimetal-semiconductor and indirect-direct band gap transitions," *Angewandte Chemie Int.* Ed., vol. 54, no. 10, pp. 3112–3115, 2015.
[9] E. Akturk, O. U. Akturk, and S. Ciraci, "Single and bilayer bismuthene: Stability at high temperature and mechanical and electronic properties," *Phys. Chem. Phys.*, vol. 94, no. 1, 2016, Art. no. 014115.
[10] M. A. McGuire et al., "Magnetic behavior and spin-lattice coupling in cleavable van der waals layered $CrCl_3$ crystals," *Phys. Rev. Mater.*, vol. 1, no. 1, 2017, Art. no. 014001.
[11] S. Yanxing, C. Changchun, F. Qingyang, Z. Wei, and Y. Yintang, "Lateral magnetic tunnel junctions with a heterointerface-induced half-metallic electrode," *J. Phys. Chem. Solids*, vol. 167, no. 1, 2022, Art. no. 110754.
[12] Atomistix Quantumwise A/S, 2021. [Online]. Available: www.quantumwise.com
[13] J. P. Perdew, K. Burke, and M. Eenzerhof, "Generalized gradient approximation made simple," *Phys. Rev. Lett.*, vol. 77, no. 18, pp. 3865–3869, 1996.
[14] H. J. Monkhorst and J. D. Pack, "Special points for brillouin-zone integrations," *Phys. Rev. B*, vol. 13, no. 12, pp. 5188–5192, 1976.
[15] V. I. Anisimov, J. Zaanen, and O. K. Andersen, "Band theory and mott insulators: Hubbard U instead of stoner I," *Phys. Rev. B*, vol. 44, no. 3, pp. 943–954, 1991.
[16] M. Qi, S. Dai, and P. Wu, "Prediction of electronic and magnetic properties in 3d-transition-metal X-doped bismuthene (X = V, Cr, Mn and Fe)," *Appl. Surf. Sci.*, vol. 486, pp. 58–64, 2019.
[17] S. M. Hailemariam et al., "Electronic structure and room temperature of 2D dilute magnetic semiconductors in bilayer MoS_2-doped Mn," *Adv. Condens. Matter Phys.*, vol. 2020, pp. 1–8, 2020.
[18] N. Mishra, B. P. Pandey, B. Kumar, and S. Kumar, "Enhanced electronic and magnetic properties of N_2O gas adsorbed Mn-doped $MoSe_2$ monolayer," *IEEE Trans. Electron. Devices*, vol. 69, no. 4, pp. 1634–1641, Apr. 2022.

[19] P. Lv, Y. L. Li, and J. F. Wang, "Monolayer Ti_2C MXene: Manipulating magnetic properties and electronic structures by an electric field," *Phys. Chem. Chem. Phys.*, vol. 22, no. 20, pp. 11266–11272, 2020.
[20] M. I. Katsnelson, V. Y. Irkhin, L. Chioncel, A. I. Lichtenstein, and R. A. de Groot, "Spin-metallic ferromagnets: From band structure to many-body effects," *Rev. Modern Phys.*, vol. 80, no. 2, pp. 315–378, 2008.
[21] M. Zhang, H. Guo, J. Lv, J. Jia, and H. Wu, "The 3d transition-metals doping tunes the electronic and magnetic properties of 2D monolayer InP_3," *J. Magnetism Magn. Mater.*, vol. 533, no. 1, 2021, Art. no. 168026.
[22] S. Choudhary and A. K. Garg, "Enhanced absorption in $MoS_2/Hg_{0.33}Cd_{0.66}Te$ heterostructure for application in solar cell absorbers," *IEEE Trans. Nanotechnol.*, vol. 18, pp. 989–994, 2019.
[23] T. Song et al., "Giant tunneling magnetoresistance in spin-filter van der Waals heterostructures," *Science*, vol. 360, no. 6394, pp. 1214–1218, 2018.
[24] G. Henkelman, A. Arnaldsson, and H. Jónsson, "A fast and robust algorithm for bader decomposition of charge density," *Comput. Mater. Sci.*, vol. 36, no. 3, pp. 354–360, 2006.
[25] B. Chettri et al., "Hexagonal boron nitride (h-BN) nanosheet as a potential hydrogen adsorption material: A density functional theory (DFT) study," *Surf. Interfaces*, vol. 24, no. 1, 2021, Art. no. 101043.
[26] Y. Song, C. Chai, Q. Fan, W. Zhang, and Y. Yang, "Magnetic tunnel junctions with a heterointerface-induced half-metallic electrode," *J. Phys. Chem. Solids*, vol. 167, no. 1, 2022, Art. no. 110754.
[27] K. L. Yao, Y. Min, Z. L. Liu, H. G. Cheng, S. C. Zhu, and G. Y. Gao, "First-principles study of transport of V doped boron nitride nanotube," *Phys. Lett. A*, vol. 372, pp. 5609–5613, 2008.
[28] M. Kan, S. Adhikari, and Q. Sun, "Ferromagnetism in MnX_2 (= S, Se) monolayer," *Phys. Chem. Chem. Phys.*, vol. 16, no. 10, pp. 4990–4994, 2014.
[29] N. Mishra, B. P. Pandey, and S. Kumar, "Impact of Mn- and Fe-doping on electronic and magnetic properties of MoX_2 (X = S, Se) monolayer," *IEEE Trans. Electron. Devices*, vol. 69, no. 3, pp. 1553–1560, Mar. 2022.
[30] Y. Yue, C. Jiang, Y. Han, M. Wang, J. Ren, and Y. Wu, "Magnetic anisotropies of Mn-, Fe-, and Co-doped monolayer MoS_2," *J. Magn. Magn. Mater.*, vol. 496, no. 1, 2020, Art. no. 165929.
[31] S. H. Hoseyni, K. Rahimi, B. Barakati, A. Sadeghi, and S. M. Mohseni, "Magnetic anisotropy in Co/phosphorene heterostructure," *Physica E: Low-Dimensional Syst. Nanostructures*, vol. 128, 2021, Art. no. 114620.